SUPPORTING INFORMATION

Quantifying Colorimetric Assays in Paper-Based Microfluidic Devices by Measuring the Transmission of Light through Paper

Audrey K. Ellerbee, [a] Scott T. Phillips, [a] Adam C. Siegel, [a,b] Katherine A. Mirica [a], Andres W. Martinez, [a] Pierre Striehl, [c] Nina Jain, [a] Mara Prentiss, [c] and George M. Whitesides [a] *

[a] *Department of Chemistry and Chemical Biology, Harvard University, Cambridge, MA 02138 USA*

[b] *School of Engineering and Applied Sciences, Harvard University Cambridge, MA 02138 USA*

[c] *Department of Physics, Harvard University, Cambridge, MA 02138 USA*

*author to whom correspondence should be addressed

ABSTRACT

We present an effective-medium theory model that describes the transmission of light through oil-wet paper, and discuss the design and performance of the transmittance colorimeter that determines the level of protein in artificial urine by measuring the transmission of light through oil-wet paper. We also present the experimental protocols relevant to fabrication of the paper-

based microfluidic devices and the plastic sleeves used for application of an index-matching fluid, as well as the procedure used to generate a calibration curve to relate the output of the colorimeter to the detected transmittance. The effects of various environmental conditions on measurement of the transmission of light through paper are also described.

THEORY AND MODEL OF THE TRANSMISSION OF LIGHT IN WET PAPER

General Transmittance Theory. Light incident on a surface corresponding to the boundary of two media (e.g., paper and air) with indexes of refraction n_1 and n_2 ($n_1 \neq n_2$), respectively, is either scattered, absorbed, or transmitted. Both forward-scattered and unscattered light contribute to the transmitted intensity. Equation S-1[1] describes the constant of proportionality τ that gives the proportion of incident light of intensity I_0 (W/cm^2) that penetrates the surface of medium 2. The values of θ for the two media are the typical angles used in refraction calculations governed by Snell's law, and the electric field amplitude transmission coefficient t depends on the polarization of I_0.

$$\tau = \left(\frac{n_2 \cos(\theta_2)}{n_1 \cos(\theta_1)} \right) t^2$$

$$\text{where } t = \begin{cases} \dfrac{2n_1 \cos(\theta_1)}{n_1 \cos(\theta_1) + n_2 \cos(\theta_2)}, & I_0^{\perp} \\ \dfrac{2n_1 \cos(\theta_1)}{n_1 \cos(\theta_2) + n_2 \cos(\theta_1)}, & I_0^{\parallel} \end{cases} \qquad \text{(S-1)}$$

Light entering a medium may be attenuated as it travels if the medium is absorbing or contains scattering particles that are large relative to the wavelength of the light. The proportion of light that is attenuated after traveling a distance z (cm) in the medium is related to the

attenuation coefficient α (cm^{-1}) of the medium (Equation S-2)[1], where α is the total linear attenuation due to absorption and scattering ($\alpha = \alpha_{abs} + \alpha_{sca}$).

$$I_{out} = 10^{-\alpha z} I_{in} \qquad \text{(S-2)}$$

In general, the scattering coefficient is a function of the wavelength-dependent scattering cross-section C_{sca} (cm^2), which is related to the geometrical cross-section of the scatterer, and of the volume density of scatterers N (cm^{-3}) in the medium. For a medium of homogeneous scatterers of different sizes, Equation S-3[2] describes this relationship, where a (cm) denotes a parameter that describes the size of the scatterer (e.g., the radius of a spherical particle) as measured in vacuum; the wavelength of the incident light in vacuum is denoted as λ (cm). Note that the equation for a scatterer embedded in a medium (of refractive index n) other than vacuum can be obtained by making an appropriate change of variables, such as $x = 2\pi an / \lambda$.

$$\alpha = \int_0^\infty C_{sca}(a) N(a) da \qquad \text{(S-3)}$$

An Optical Model for Paper. For simplicity, we adopt an effective-medium model in which we consider the paper as a collection of randomly-oriented, homogeneous scatterers (that is, fibers with uniform scattering properties) of different sizes separated by large voids (ordinarily, air). Without loss of generality, we can model the paper alternatively as a porous medium of polydispersed scatterers (e.g. paper fiber) of refractive index n_p in a continuous fluid medium (e.g., air) of refractive index n_f, as shown in Figure S-1A. We define the quantity ϕ, where $0 \leq \phi \leq 1$, as the total volume fraction (v.f.) of paper fiber in the bulk material. We can then apply volume averaging theory to define an effective refractive index (n_{eff}) for the paper[3] (Equation S-4), which is easily seen to tend to n_f and n_p for the extreme cases $\phi = 0$ and $\phi = 1$,

respectively (Figure S-1B). The term κ is defined as the degree of index matching between the paper fibers and the surrounding fluid.

$$n_{eff} = n_p \sqrt{\phi + (1-\phi)\frac{n_f^2}{n_p^2}} = \kappa n_p \qquad \text{(S-4)}$$

Equations S-1 and S-2 can be used together to describe the total transmission of light through paper, where the media 1 and 2 are replaced by air (n_{air}) and paper (n_{eff}), respectively. We limit our remaining discussion to the case where the air, paper, and index-matching fluid are non-absorbing, noting that absorption by any of these mediums is a separable effect that results in attenuation of the total light by a factor related to the absorption coefficient of the absorbing medium (e.g. analyte, urine sample), as given in Equation S-2.

The Effect of a Colorimetric Assay on Transmission Through Paper. After a colorimetric assay, the transmission of light through paper is attenuated relative to the case for a non-assay due to absorbance of the dye (and possibly also scattering by the molecules of dye) produced during the assay. This additional attenuation is described by the Beer-Lambert law (Equation S-5). Here, ε ($M^{-1}cm^{-1}$) is the molar extinction coefficient of the dye, c (M) is the concentration of the dye, and z (cm) is the optical path length of the paper. The magnitude of this extinction constitutes our signal of interest.

$$I_{out} = I_{in} 10^{-\varepsilon c z} \qquad \text{(S-5)}$$

To find the total transmission from the source to the detector, we must take into account the boundary transmission factors described by Equation S-1 for the air-paper and paper-air boundaries of our model, as well as the attenuation within the paper described by Equation S-2. Assuming lossless travel through air (i.e., no scattering), Equation S-6 relates the final intensity I (W/cm^2) at the detector after a colorimetric assay to the source intensity I_0; here α_{samp} (cm^{-1})

accounts for attenuation (both scattering and absorption) caused by the sample (e.g. urine), α_{sca} (cm^{-1}) is the scattering coefficient of the paper, and τ_{in} and τ_{out} (both unitless) correspond to the transmission coefficients for the air-paper and paper-air interfaces, respectively (note that although the media are the same in both cases, the transmission coefficients may differ depending on the polarization effects of the paper, even for incident light of a single linear polarization). We call the variable T_c (unitless) the characteristic transmittance of the paper, which is the transmittance of the paper in the absence of an applied sample or colorimetric test.

$$I = \tau_{in} 10^{-\alpha_{sca} z} 10^{-\alpha_{samp} z} 10^{-\varepsilon c z} \tau_{out} I_0 = T_c 10^{-\alpha_{samp} z} 10^{-\varepsilon c z} I_0 \qquad \text{(S-6)}$$

When within the limits of detection of the electronics of the detector of choice, the largest relative change in transmittance before and after the colorimetric assay occurs when attenuation is dominated by light extinction by the dye, rather than by scattering in the paper; this fact suggests that T_c should be maximized to maximize sensitivity to the analyte. Consider a detector with a finite instrument detection range that can detect light with intensities in the range I_{min} to I_{max}: the instrument detection range is I_{max} - I_{min}. The corresponding method detection range (MDR) of a colorimetric assay performed using this system is given by Equation S-7, where the functions min(x,y) and max(x,y) denote, respectively, the minimum or maximum values of their arguments. The method detection range of the assay (the highest and lowest concentrations of dye one can reliably measure) is, at best, given by Equation S-8, where c_0 is the concentration of dye corresponding to the lowest detectable intensity of transmitted light, and represents an upper limit on the detectable concentration. Since $T_c \leq 1$, Equation S-8 implies that, for paper of a given thickness, decreasing T_c will enable the measurement of higher concentrations of dye but will limit the sensitivity of the system (as defined by the magnitude of the detected change in signal relative to a non-assay) to lower concentrations; conversely, for paper with a given characteristic

transmittance, increasing z (by using a thicker piece of paper, for example) will increase the observed sensitivity to lower concentrations of dye, but will limit the maximum concentration that can be detected. Thus, the discrimination of low concentrations is best enabled when T_c is maximized. Note that because of the fixed instrument range of the system, there is a tradeoff between T_c, I_0, and z with respect to c_0 (Equations S-7, S-8).

$$MDR = \min(I_{\max}, T_c 10^{-\alpha_{samp} z} I_0) - \max(I_{\min}, T_c 10^{-\alpha_{samp} z} 10^{-\varepsilon c_0 z} I_0) \quad \text{(S-7)}$$

$$MDR_{\max} = T_c 10^{-\alpha_{samp} z} I_0 (1 - 10^{-\varepsilon c_0 z}) \quad \text{(S-8)}$$

The Effect of Index-Matching on Transmission Through Paper. For paper of a given optical path length (z), n_p, and ϕ, our goal is to maximize the sensitivity of paper to extinction during a colorimetric assay by maximizing its characteristic transmittance. This sensitivity enhancement can be achieved in two ways: (i) by minimizing scattering in the paper (governed by the Beer-Lambert law) and (ii) by maximizing the transmission coefficients τ_{in} and τ_{out} at the interfaces of the paper (governed by Snell's law).

Revisiting Equation S-3, we note that the scatterers of our paper model are embedded in a fluid of refractive index n_f, so a change of variables is appropriate. The effect of this change can be understood by carrying out the following thought exercise. Let us assume the scattering particles are of arbitrary size, shape, arrangement, and size distribution. Our main interest is in the general dependence of the scattering cross-section on n_f. We adopt as the starting place for understanding light boundary effects (in this case, for a single scattering event) Snell's law, since the boundary is intrinsically defined as the location of a refractive index mismatch. From this vantage point, it is clear that the instantaneous scattering is related to reflectance[4] since, by conservation of energy and conservation of momentum, light that is not transmitted (i.e., refracted) or absorbed is reflected at a deviation angle related to the angle of incidence and the

relative refractive index of the two interfacing media. Hence, while it is obvious that perfect index-matching ($n_f = n_p$, κ=1) eliminates scattering altogether, this fact is also born out by noting the vanishing reflectance coefficient of the light as n_f/n_p tends to 1 from both directions (Figure S-2A), regardless of the incident angle or polarization state. Note that the volume fraction is related to N (cm^{-3}) by Equation S-9, where mw_p and ρ_p are the molecular weight and density, respectively, of the paper fibers, and N_A is Avagadro's number, and that the scattering cross-section diminishes as $n_f \rightarrow n_p$. Therefore, α_{sca} can be recast as a function of κ (not shown) assuming that C_{sca} is known.

$$\phi = N * mw_p / N_A \rho_p \tag{S-9}$$

The dependence of the transmission of light through paper due to the extent of permeation of the index-matching fluid can be accommodated by extending our optical model of paper to include a dispersed phase (n_{air}) with a time-dependent volume fraction $\varphi(t)$, $0 \leq \varphi(t) \leq 1$, where the constant n_f term in Equation S-4 is replaced by the time-dependent Equation S-10. Here, $\varphi(t) \rightarrow 1$ or 0 as $t \rightarrow 0$ or ∞, respectively. Technically, the expression for the scattering coefficient (Equation S-1) should also be modified to consider a time-dependent change in transmission at air-fluid boundaries (as opposed to paper-fluid or paper-air) as the air is displaced; the role of τ (defined by Snell's law) in determining the overall transmittance increases as we approach the perfect index-matching condition.

$$n_f(t) = \varphi(t) n_{air} + (1 - \varphi(t)) n_f \tag{S-10}$$

Thus, minimizing scattering within the paper is not sufficient to maximize the characteristic transmittance. Equation S-1 reminds us that the total transmission through paper is also related to attenuation at the air-paper interfaces, for which the relevant refractive indexes are that of air and the effective refractive index of the bulk paper-fluid complex. We can modify the

effective refractive index of paper – or equivalently, modify the degree of index mismatch of paper of a given v.f. – by changing the refractive index of the constituent fluid surrounding the paper fibers (i.e., by wetting the paper with an index-matching fluid). (Figure S-2B). For dry paper, n_f is simply the index of refraction of air. Equation S-1 can be plotted a function of κ (Figure S-2B); it is notable that the maximum value of τ does not necessarily occur at the perfect index-matching condition ($\kappa = 1$).

Hence, to maximize total transmission of light for a given paper type, one must determine the value of n_f that corresponds to the optimal value of κ that simultaneously maximizes τ and minimizes α_{sca}. Because τ is a function of the incident angle (and polarization state), in practice one could use the average value of τ over the acceptance angles of the assay area and detection area to carry to the optimization. An exact analytical expression for the dependence of α_{sca} on n_f can only be obtained for the simplest of cases (e.g., for homogeneous spheres using Mie theory), but could be determined experimentally.

We expect, as per our previous discussion, that reflectance at a boundary is minimized (i.e., transmission is maximized) when the boundary indexes (n_{air} and n_{eff}) are nearly matched; it moreover follows that for two papers with different constituent fibers that are index-matched to the same degree (i.e., $\kappa_1 = \kappa_2$), transmission will be higher for the paper whose constituent fibers have a lower refractive index (that is, as n_p approaches n_{air}) since its effective refractive index is more closely matched to air.

Increasing the Dynamic Range of a Colorimetric Assay. The use of a control assay carried out in parallel with the real assay allows us to cancel all effects not related to absorption of the dye (e.g., scattering and absorption by the paper, fluid, or sample), thereby isolating our output to the signal of interest. This normalization is done by taking the ratio of the intensity of a

colorimetric assay (I_{ASSAY}) to that of a control assay ($I_{CONTROL}$: paper, matching fluid, and sample, but none of the reagent used to generate the specific colorimetric response) (Equation S-11). For the same output intensity, the normalization process instantaneously increases the dynamic range of the assay by a factor $1/I_{CONTROL}$. The precision of the result is, however, further limited, in this case, by the noise associated with inhomogeneities in the paper (e.g., local variations in n_p, z). Electronic noise, such as thermal noise and Schottky noise, sets the lower limit on I_{min}.

$$T_N = I_{ASSAY} / I_{CONTROL} = 10^{-\varepsilon c z} \qquad \text{(S-11)}$$

EXPERIMENTAL

Fabrication of the μ-PAD.

Fabrication of the paper-based microfluidic device. Microfluidic features were patterned into Whatman Chromotography Paper No. 1 using photolithography, as described previously.[5, 6] The entire μ-PAD is ~12.5 mm × 22.7 mm × 0.11 mm; the area for running assays is ~12.5 mm × 13.7 mm × 0.11 mm and the photoresist tab has dimensions of 12.5 mm × 9 mm × 0.11 mm. There is a 4.2-mm-diameter hole located 1.3 mm and 4.1 mm from the top and sides of the device, respectively to match the diameter of the posts in the transmittance colorimeter.

Four circular hydrophilic regions of 2-mm diameter are arranged in a square pattern in the center of the device (i.e., 2.5 mm from the outer edge of the device). One of the circles is for measuring $I_{CONTROL}$ (labeled 'CONTROL' on the device), the other three are for assays (labeled '1', '2', and '3'). Each circle can be individually read by mounting the paper in the holder and aligning the hole with the post corresponding to the assay of interest (Figures 3C and 3D). Reading a subsequent circle can be accomplished by removing the paper, turning it clockwise by

90°, and re-inserting it into the holder. The labels are oriented so that the text corresponding with the assay region being read appears upright.

Fabrication of the plastic sleeves. The sleeves were made of 1.0-mil plastic drop cover (ACE Hardware) that was obtained as a single sheet (9' x 12') from a local hardware store. Sheets of plastic drop cover were cut to a manageable size (~8.5" x 11") and patterned with an array of perpendicular lines using a plastic sealer (AIE-300 Impulse Sealer, American International Electric). The interior dimensions of the sleeves were slightly larger than the dimensions of the paper microfluidic devices (14 mm × 14 mm), and the exterior dimensions (15 mm^2) were sized to fit into the aluminum holder (Figure 3B). Individual sleeves were cut from the sealed plastic matrix using scissors; each sleeve was sealed on three sides and contained one open end.

Fabrication and Operation of the Transmittance Colorimeter.

The electronic circuit diagram for the colorimeter is given in Figure S-3. All electronic components used in the transmittance colorimeter were purchased from an electronics supply catalog (Digikey Inc.). The circuit comprises eleven active electronic components: an oscillator circuit (LM393, National Semiconductor Inc.), a tri-color LED source (425-1818, Sharp Inc.), an internally-amplified phototransistor (IS455, Sharp Inc.), two electronic filters (UAF42, Texas Instruments Inc.), a low-power electronic amplifier (LM6041, National Semiconductor Inc.), an analog to digital converter (ICL7106, Intersil Inc.), a 3.5-digit numerical liquid crystal display (VI-301, Varitronix Inc.), a voltage inverter (UA7800, Texas Instruments Inc.), and a voltage regulator (ICL7600 Intersil Inc.). The circuit also uses 5 potentiometers, 41 surface-mount resistors and capacitors, a bipolar junction transistor (2N4403, Motorola Inc.) and a single junction diode (1N4148, Fairchild Semiconductor Inc.).

Briefly, a 9-V alkaline battery provides power to a voltage inverter, which converts the 9-V DC input into a ±9-V supply. A voltage regulator converts the ±9 V to a ±5 V supply that powers all components in the circuit. The light generator consists of a frequency selector connected to a laser diode driver, which is connected to a switchable tri-color LED (630 nm, 525 nm, and 470 nm). The light from the LED, modulated at 1 kHz to make it easily distinguished from ambient light (such as sunlight), passes through a region in the paper relevant to an assay. Modulation is accomplished via a programmable timer/oscillator IC. We chose a tri-color LED over a white LED to eliminate the need to filter wavelengths of light not used in a given assay. By selecting the color of the LED to use for detection based on the color produced in an assay (for example, we use the red LED for assays that produce a blue color), we can increase the sensitivity of detection (by selecting the wavelength option that provides the greatest extinction for a given assay). This wavelength selectivity feature also makes it possible to use the same detection device to perform different colorimetric assays.

The light transmitted through the paper is detected using an integrated circuit (IC) incorporating a phototransistor, whose output is amplified by an electronic amplifier. This amplified signal passes through a 1-kHz bandpass filter to a peak detector (comprising a second op-amp coupled to a diode) that converts the amplitude of the periodic signal to a direct current (DC) signal. This DC signal then passes through an analog-to-digital converter, which converts its input voltage into a set of digital signals that illuminate a matching 3.5-digit numerical liquid crystal display (LCD).

The device is able to accommodate a variety of mounts designed to fit different shapes and thicknesses of samples and light source–photodetector pairs. For the experiments in this paper, we used a two-piece aluminum mount (manifold) with dimensions that match the

dimensions of the μ-PAD. The top block of aluminum contained a space for aligning and securing the light source (LED), and a hole (radius = 1 mm), through which light passed to reach the paper. The bottom block of aluminum contained a corresponding hole (radius = 1 mm), through which light passed from the paper to reach the light detector, and a space for aligning and securing the source LED. The bottom of the holder also includes posts that match a hole punched in the μ-PAD; these posts serve to orient the device so that only the circular detection zone of interest aligns with the optical components of the colorimeter (Figures 2B and 3D). When the device and holder are machined and mounted correctly, the closed holder blocks ambient light.

We glued into the holder and onto the lid, 120-μm-thick pieces of black transparency[7] with a 1.5 mm-diameter hole removed in the region covering the IC detector and a 5 mm-diameter hole removed over the LED. The black transparency in the holder serves as a spatial filter or aperture stop that prevents scattered light that passes from the LED through the surrounding photoresist (i.e., light incident on regions other than the detection zones) from reaching the detector. The black transparency on the lid (~17 mm^2) compresses the μ-PAD when the lid is closed, and holds the device flat during transmittance measurements. The transparencies are also easy to clean or change, which facilitates cleanup of the colorimeter.

The device can operate continuously for ~5 h on a single 9V battery; this power requirement limits the system lifetime. Other components of the system (LEDs, LCD display, solid-state electronics) have typical mean times between failures (relevant for reparable equipment) or mean times to failure (for irreparable parts) on the order of 30,000 – 750,000 hours or more for continuous operation. The system casing (which is currently aluminum, but

undoubtedly could be made of injection-molded or stamped polymer in larger-scale production, to lower both cost and weight) does not contribute to the lifetime of the system.

The total cost of the receiver electronics was ~$30, and that of the overall device was ~$50. The former figure could be reduced by up to 30% by redesigning the electronic filter using simpler electronic components; we can achieve substantial reduction of the latter by replacing the discrete components with a single integrated circuit (IC) and manufacturing this IC at large volume.

Total Protein Assay.

The μ-PADs were prepared for the protein assay by depositing 0.5 μL of a citrate buffer solution (pH 1.8) into the three circular detection zones. The paper was allowed to dry at 23 °C, after which time we deposited 0.5 μL of a 9-mM tetrabromophenol blue solution in ethanol into the detection zones, and dried the paper again at 23 °C for at least two hours.[8] The microfluidic devices were dipped into vials containing solutions of bovine serum albumin (BSA) in artificial urine for 1 s to a depth sufficient to cover all of the detection zones simultaneously (~13 mm, approximately to the hydrophilic line demarcating the tab in Figure 3A); excess urine was removed from the device by grazing the front and back one time each against the edge of the vial.[9] Tetrabromophenol blue responded immediately to BSA in the sample. We let the devices dry at 23 °C for an additional 6-12 min.

We applied vegetable oil (the index-matching fluid) to the device by adding 15 μL of the fluid to a plastic sleeve and inserting the μ-PAD into the sleeve. We gently smeared the fluid in the sleeve over the detection zones by rotating the thumb and forefinger over the sleeve/device combination for 3 s. The vegetable oil was allowed to absorb into the detection zones for ~ 12-15 min before making measurements.

Generation of a Calibration Curve for Protein Measurements

A calibration curve (using the 630-nm LED) (Figure 4) relating the concentration of protein in artificial urine to T_N was generated for microfluidic devices containing tetrabromophenol blue. The μ-PADs were dipped into samples of BSA in artificial urine of known concentrations for ~one second, grazed across the side of the vial to remove excess urine, and inserted after one minute into plastic sleeves containing 15 μL of vegetable oil. The devices were left to absorb the vegetable oil for at least 12 minutes before measuring their transmittance using the handheld colorimeter. Three devices were used for each condition, giving nine total repetitions per sample.

OPTICAL DEVICE CHARACTERIZATION AND PERFORMANCE

Calibration of the Colorimeter. The optical detector contains five potentiometers (variable resistors) that allow the circuit to be adjusted to detect a broad range of signals. These potentiometers allow for adjustment of: (i) the modulation frequency of the light source, (ii) the frequency selected to pass through the electronic band-pass filter IC, (iii) the bias voltage of the tri-color LED, (iv) the bias voltage of the phototransistor, and (v) the dynamic range of the analog-to-digital converter. The last of these potentiometers allows the user to calibrate the visual display to show a maximum value of 1999 (over a range of 0 – 1999) for the sample that corresponds with maximum transmission.

Colorimeter Performance in Various Lighting Conditions. Frequency modulation provides a simple and adaptable method for performing highly sensitive detection at minimal cost. To characterize the benefit of modulation, we passed light through a sheet of clear, transparent glass (1 cm × 1 cm × 700 μm) at five frequencies (0 Hz, 10 Hz, 100 Hz, 1 kHz, 10 kHz) and under

four lighting conditions (dark room, indoor fluorescent, outdoor shade, outdoor direct sunlight). For these measurements we used a modified manifold in which the light source and receiver were separated by 5 cm; this separation exposed the phototransistor to ambient light. For each frequency and lighting condition, we recorded the signal-to-noise ratio as the ratio of the number observed in the display with the light source turned on (signal) to the number observed in the display with the light source turned off (noise).

All modulated signals (frequency ≥ 10 Hz) had signal-to-noise ratios comparable to the ratio observed for the un-modulated signal (frequency = 0 Hz) obtained in the dark room; there was no observable dependence of the signal-to-noise ratio on the frequency itself. Un-modulated signals measured under indoor fluorescent lamps, outdoors in the shade, and outdoors under direct sunlight gave much lower signal-to-noise ratios (e.g., as low as 1:1 depending on the strength of the light) than those observed with modulated signals (e.g., up to 200:1)**.**

Measuring Opacity: We purchased neutral density optical filters (100% SiO_2, 700 μm × 1 cm × 1 cm) of varying transmission coefficients (0.80, 0.63, 0.50, 0.40, 0.32, 0.25, 0.10, 0.05, 0.01) from an optical supply catalog (Edmund Industrial Optics, Inc.) (Figure S-4). The signal generated by light from the red LED was permitted to settle for 30 s before recording the number displayed in the LCD. We repeated the experiment for the other glass filters and also for the green and blue LEDs. This experiment verifies that the optical detector can be used to quantify the opacity of a sample by measuring the amount of light that passes through it.

Quantifying Color. The colorimeter can quantify the color of a sample by measuring transmittance of light at three distinct wavelengths: red (630 nm), green (525 nm) and blue (470 nm). We measured the colorimetric profile of six optical bandpass filters (red, green, blue, yellow, cyan, and magenta, Edmund Industrial Optics, Inc.) in the colorimeter using a multi-step

process: we turned on the red LED and allowed the signal to settle for 30 s before recording the number displayed on the LCD; we then repeated this process for the green and blue LEDs. This procedure generated a unique RGB "profile" of the sample comprising three numbers (an R-value, G-value, and B-value), each describing the intensity of light from that particular colored source that passed through the sample as a number from 0-1999 (the maximum number displayable on the LCD) (Figure S-5). Samples that transmitted red light produced RGB profiles with elevated R-values (R = 1397), and diminished G- and B-values (G = 6, B = 6), as expected. We used a modulation frequency of 1 kHz for all measurements. Using these profiles, it is possible to use the portable detector to detect colors quantitatively in a broad range of wavelengths in the visible spectrum.[10]

Comparison with a Commercial Colorimeter: We used a commercial spectrophotometer (8453 UV-Vis, Hewlett-Packard Inc.) to measure the intensity of light that passed through each sample as a function of wavelength for comparison with the results obtained using the handheld colorimeter (Figure S-5). While the commercial device provides the full visible spectrum between 400 nm and 700 nm that passes through a sample, the RGB profile obtained from the handheld colorimeter produces sufficient information to discriminate between a variety of colors. At steady state, the maximum fluctuation (error) in the readout for each color was ±2 digits or 0.27% at high numeric values (~1600), and ±0.5 or 0.5% at low numeric values (~100). Assuming an average error of 0.4%, the detector can, in principle, discriminate ~250 levels for each color, which corresponds to a total of $(250)^3$ = 15,625,000 unique color combinations.

METHOD CHARACTERIZATION AND PERFORMANCE

Effect of Wetting Time. We measured the rate at which vegetable oil renders Whatman chromatography paper No. 1 translucent by placing a 10-mm × 7-mm piece of paper over the optical IC detector in the colorimeter and by applying a 15-μL drop of vegetable oil in the center of the paper; the 15-μL drop mimics the vegetable oil distributed to the device by the plastic sleeve. We recorded *I* over time until the transmission reached steady-state. The experiment was conducted in a room with controllable temperature and humidity, at a temperature of 31°C and a relative humidity of 21%.

When the vegetable oil was applied to the paper, the intensity of light transmitted through the paper increased instantaneously – *T* increased from 0.19 to 0.44 within the first 30 seconds, and then increased gradually over the next ~8 min, reaching a steady state after ~ 10 min (Figure S-6, solid black line). The decrease in transmittance observed at ~7 min is possibly due drift in the electronic readout (over the course of the experiment, I_0 decreased to 98.4% of its original value), although this feature did not appear consistently in other data sets subject to drift. The changing value of the transmittance over time can be partly explained by an optical model of paper that includes a dispersed phase (n_{air}) with a time-dependent volume fraction (see "Theory and Model of the Transmission of Light in Wet Paper"). We found that some scattering persists even after long wetting times due to residual air bubbles that have been trapped in the paper; evacuating oil-wet paper to 0.5 Torr yields about a 10% increase in transmittance (data not shown).

Effect of Temperature (Viscosity). We repeated the wetting-time experiment at higher room temperatures (26°C and 36°C) and the same humidity (RH = 20%) (Figure S-6A). The application of the index-matching fluid caused an immediate increase (within 30 seconds) in

transmittance. For all temperatures investigated, the transmittance measured at 30 seconds was greater than or equal to 92% of the final, steady-state transmittance. The variability in detector drift between experiments (I_0 decreased by 1.6%, 7.0%, and 4.1% for temperatures of 26°C, 31°C and 36°C, respectively, over the course of the experiment) prevents a direct comparison of the three datasets; we hypothesize, however, that the time to reach steady state would be shorter in a drift-less system in a higher temperature environment. The viscosity of the index-matching fluid is related to the rate at which it is absorbed by the paper, and the known effect of temperature on viscosity suggests that temperature would play a role in influencing the rate of absorption, and, consequently, transmittance. In our system, steady-state transmittance is achieved after 10 minutes regardless of the temperature, with higher temperatures appearing to reach steady state more quickly.

Effect of Relative Humidity. Repeating the wetting-time experiment described previously at constant temperature and varying conditions of relative humidity (RH = ~21%, 36%, and 66%) yielded the traces found in Figure S-6B. As with the previous experiment, detector drift also varied for different experimental conditions (I_0 decreased by 7.0%, 2.5%, and 7.1% for relative humidities of 21%, 36%, and 66%, respectively, over the course of the experiment), although a comparison of the two extreme humidity conditions tested (whose magnitudes of detector drift were nearly equivalent) shows that a higher steady state transmittance is attained for the higher humidity condition. The higher observed transmittance for the high humidity condition may be explained by the higher water content in the air: not only is the refractive index of the humid air better matched to that of the oil-wet paper (since water has a higher refractive index than air, yielding a higher effective refractive index for humid air), but the water content in the paper itself may also contribute to a smaller scattering cross-section for the paper (i.e., there

is likely less scattering in the paper between the paper-fibers and any residual humid air gaps that are not filled by the oil). The application of the index-matching fluid caused an immediate increase (within 30 seconds) in transmittance to greater than 92% of the final, steady-state value for all for all humidities investigated. The system reached a steady state output within 5 minutes regardless of the humidity, with the time to reach steady state appearing slightly shorter for higher humidity conditions.

Effect of Paper Thickness. We wet four 10-mm × 7-mm pieces of Whatman chromatography paper No. 1, each with 20 μL of vegetable oil, and allowed the oil to absorb into the paper for 15 min. We measured T_c for a single piece of paper, and then for stacks of sequentially increasing numbers of paper that we pressed together with the flat end of a spatula and held in place for 3 min. As the thickness of the paper stack increased, the light transmitted through the paper decayed exponentially, as is expected from Equation S-5. The transmittance decreased approximately 1.4-fold for every piece of paper added to the stack (Figure S-7). The value of α as determined from a best fit of the data is 43 cm^{-1}.

Effect of Fluid Refractive Index. We quantified the ability of several fluids to match the index of refraction of Whatman chromatography paper No. 1 (Table S-1) by applying 20-μL drops of each fluid to 10-mm × 7-mm pieces of paper, waiting 20 min for the fluid to absorb fully into the paper, and measuring the intensity of light transmitted through the paper using the handheld colorimeter. The index of refraction of Whatman chromatography paper No. 1 is 1.54–1.62[11] and fluids with indices of refraction near to this range render the paper more transparent than fluids further from this range (e.g., poly(dimethylphenylsiloxane), n = 1.536, renders the paper ~60% transparent, in contrast with distilled water, n = 1.340, which yields a transmittance of ~30%).

Effect of Paper Type. The index-matching capacity of a paper-fluid pair depends on the refractive index of the fluid and of the paper. We examined several combinations of fluids and papers to determine pairs that form transparent matrices (Table S-1). For these examples, we applied 20 μL of fluid to 10-mm x 7-mm sections of paper and waited ~40 min (to ensure that both thick and thin papers had absorbed fluids fully) before measuring the intensity of light transmitted through the paper.

Transmission through paper, described by the parameter T, depends on the type and thickness of paper: thin paper becomes more translucent than thick paper (e.g., Whatman chromatography paper No. 1 vs. No. 3) when wet with poly(methylphenylsiloxane) ($T = 0.57$ and 0.2, respectively); both Scott Roll Towels and VWR Light-Duty Tissue Wipers become more transmissive when wet with vegetable oil or poly(methylphenylsiloxane) than do the Whatman chromatography papers. The higher transmittance for the towels and wipers could be due to differences in the porosities, thicknesses or the refractive indexes of these papers that favor higher transmittance; true comparison of the absorptive quality of the two papers requires knowledge of their molar absorptivities. An effective molar absorptivity for a given paper-fluid combination could be calculated using an experiment similar to that described for Figure S-7.

The unusually high transmittance values ($T > 1$) obtained for these latter papers merit short comment: at least two explanations are plausible. First, we hypothesize that the measurement is subject to an inherent systematic error of the detector: a piece of black transparency, used as a spatial filter to block scattered from non-detection zones (Figure 2B), serves as both the entrance and exit pupil of the optical system when there is no paper is in the holder. The presence of this aperture stop leads to consistent under-measurement of I_0 relative to when another material (e.g. paper, which may have some finite focusing power) is in the

colorimeter, leading to possibly inflated values of T (since I_0 appears in the denominator). Second, given that the light source and photodetector are both protected by a set of transparencies separated by an air gap, the transmittance for the the transparency-index-matched paper boundary may be higher than for the transparency-air boundary, leading to more light incident on the detector when the paper is present. This phenomenon follows from the discussion of boundary effects on transmission given previously and depicted in Figure S-2B.

REFERENCES

(1) Hecht, E. *Optics*, 4 ed.; Addison Wesley: Boston, 2002.
(2) Van de Hulst, H. C. *Light scattering by small particles*; John Wiley & Sons, Inc: New York, 1957.
(3) Braun, M. M.; Pilon, L. *Thin Solid Films* **2006**, *496*, 505-514.
(4) Formal scattering theory seeks to explain the scattering effects of a particle of arbitrary size and geometry. The derivation usually begins by solving Maxwell's equations, taking into account the boundary conditions imposed by the existence of the particle and influenced by the shape of the particle. A complex scattering coefficient may be obtained by integrating the resulting scattering function over the geometric area of the particle, from which one may define an effective scattering cross-section and scattering efficiency for particles of a given size and shape. For example, Mie theory is dedicated to such a derivation for spheres of arbitrary size. In the present discussion, we are concerned primarily with the effect of the refractive index of the medium surrounding the scatterers on the instantaneous scattering event, rather than the full details related to computing the scattering cross-section of a particle.
(5) Martinez, A. W.; Phillips, S. T.; Wiley, B. J.; Gupta, M.; Whitesides, G. M. *Lab. Chip.* **2008**, *DOI: 10.1039/b811135a*.
(6) Martinez, A. W.; Phillips, S. T.; Whitesides, G. M. *Proc. Natl. Acad. Sci. U S A* **2008**, *105*, 19606-19611.
(7) 3M transparency film for ink jet printers (CG3460) with black ink printed on one side.
(8) Treated paper can be stored, when covered with foil, for at least 60 days before running the assay.
(9) Although this method did not control for the amount of sample used from one device to another, the detection zones for a given μ-PAD, are designed to perform sample measurements in triplicate; all zones received equal volumes of sample. Alternatively, the device can be designed with a wicking channel to uptake small volumes of sample and to better control the amount of sample reaching each detection zone.
(10) Yoshi, O. *CIE Fundamentals for Color Measurements* In *IS&T NIP16 International Conference on Digital Printing Technologies*: Vancouver, Canada, 2000.

(11) *Polymer Handbook, Fourth Edition*, Fourth ed.; John Wiley & Sons, Inc: Hoboken, New Jersey, 1999.

FIGURE CAPTIONS

Figure S-1. An optical model for describing transmittance in paper. **A**) Schematic rendering of the imaging system: light of intensity I_0 at the source plane illuminates the paper sample after traveling through air; the intensity of light exiting the sample (I) is measured at the detection plane. The paper is modeled as a porous medium whose bulk refractive index (n_{eff}) is a function of the indexes of refraction of the paper fibers (n_{p}) and the surrounding fluid or gas (n_{f}), and the paper volume fraction (v.f.) ϕ. **B**) Plot of the refractive index mis-match parameter κ from Equation S-4 as a funtion of $n_{\text{f}}/n_{\text{p}}$ for different v.f. (values 0 to 1). The perfect index-matching condition is given by $\kappa = 1$ (i.e., $n_f = n_{\text{p}}$).

Figure S-2. A) Plot of the coefficient of reflectance for parallel- (dashed) and perpendicularly- (solid) polarized light incident on a fluid-paper fiber scattering boundary as a function of the ratio of the two indexes of refraction for various angles of incidence. Note that the reflectance (and, therefore, scattering) goes to zero as we approach perfect index-matching, independent of the incident angle. **B**) Plot of the coefficient of transmittance for parallel- (dashed) and perpendicularly- (solid) polarized light incident on the boundary of two media (e.g., air and paper) as a function of the degree of index mismatch of the paper (here, $n_{\text{p}} = 1.4$) for various angles of incidence. The index-matching condition corresponding to the highest transmission ($T = 1$) depends on the angle of incidence, and does not necessarily concur with the condition of perfect index-matching (red, dashed line).

Figure S-3. Circuit diagram for the handheld colorimeter.

Figure S-4. Characterization of the opacity of a sample. The numerical output of the colorimeter at red (630 nm), green (525 nm), and blue (470 nm) wavelengths as a function of the percent of transmission of seven neutral density grayscale filters (shown at top of the image). Error bars describe the full range of the numerical output of the detector over the course of 1 min and are <1% the value of the signal. The jagged profile likely reflects the true transmittance of the optical filters because it follows the same pattern at all wavelengths.

Figure S-5. Colorimetric profiling. Photographs of six additive/subtractive optical filters (left), their corresponding spectra obtained by a commercial spectrophotometer (center), and their corresponding RGB profiles obtained by the portable colorimeter (center). Error bars describe the full range of the numerical output of the detector over the course of 1 min; for each color, the maximum observed fluctuation in the output signal (error) was <0.5%.

Figure S-6. Effect of wetting time on the transmittance ($T = I/I_0$) through Whatman chromatography paper No. 1 when wet with vegetable oil for different **A)** temperature and **B)** humidity conditions.

Figure S-7. Effect of thickness of paper (z) on the intensity of light transmitted through Whatman chromatography paper No. 1 when wet with vegetable oil. Transmitted light ($T = I/I_0$) as a function of paper thickness (z). Values represent the averages and standard deviations from seven measurements.

Figure S-1.

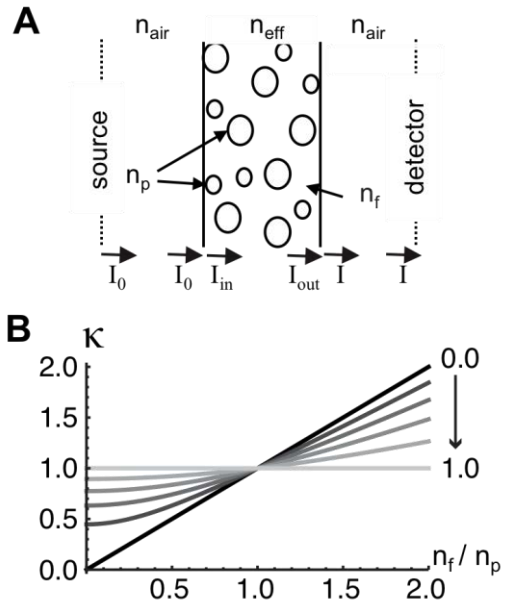
A
n_air
n_eff
n_air
source
detector
n_p
n_f
I_0
I_0
I_in
I_out
I
I
B
κ
2.0
1.5
1.0
0.5
0.0
0.0
1.0
0.5
1.0
1.5
2.0
n_f / n_p

Figure S-2.

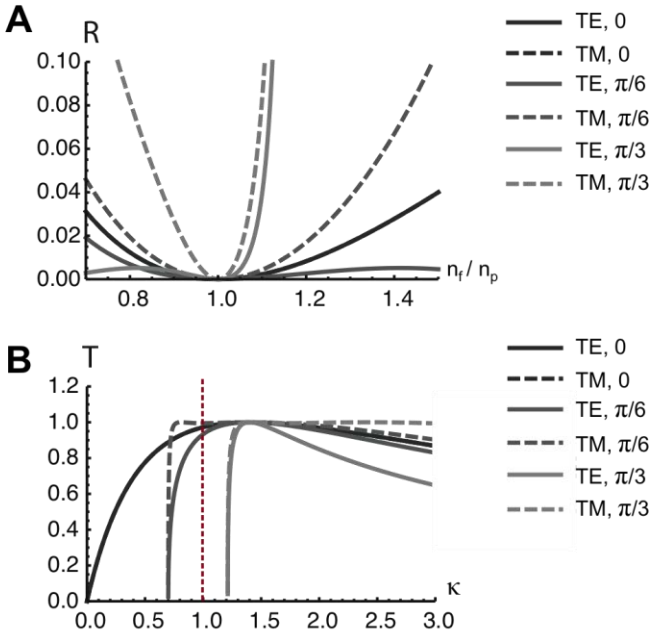
A
R
0.10
0.08
0.06
0.04
0.02
0.00
0.8
1.0
1.2
1.4
n_f / n_p
TE, 0
TM, 0
TE, π/6
TM, π/6
TE, π/3
TM, π/3
B
T
1.2
1.0
0.8
0.6
0.4
0.2
0.0
0.0
0.5
1.0
1.5
2.0
2.5
3.0
κ
TE, 0
TM, 0
TE, π/6
TM, π/6
TE, π/3
TM, π/3

Figure S-3.

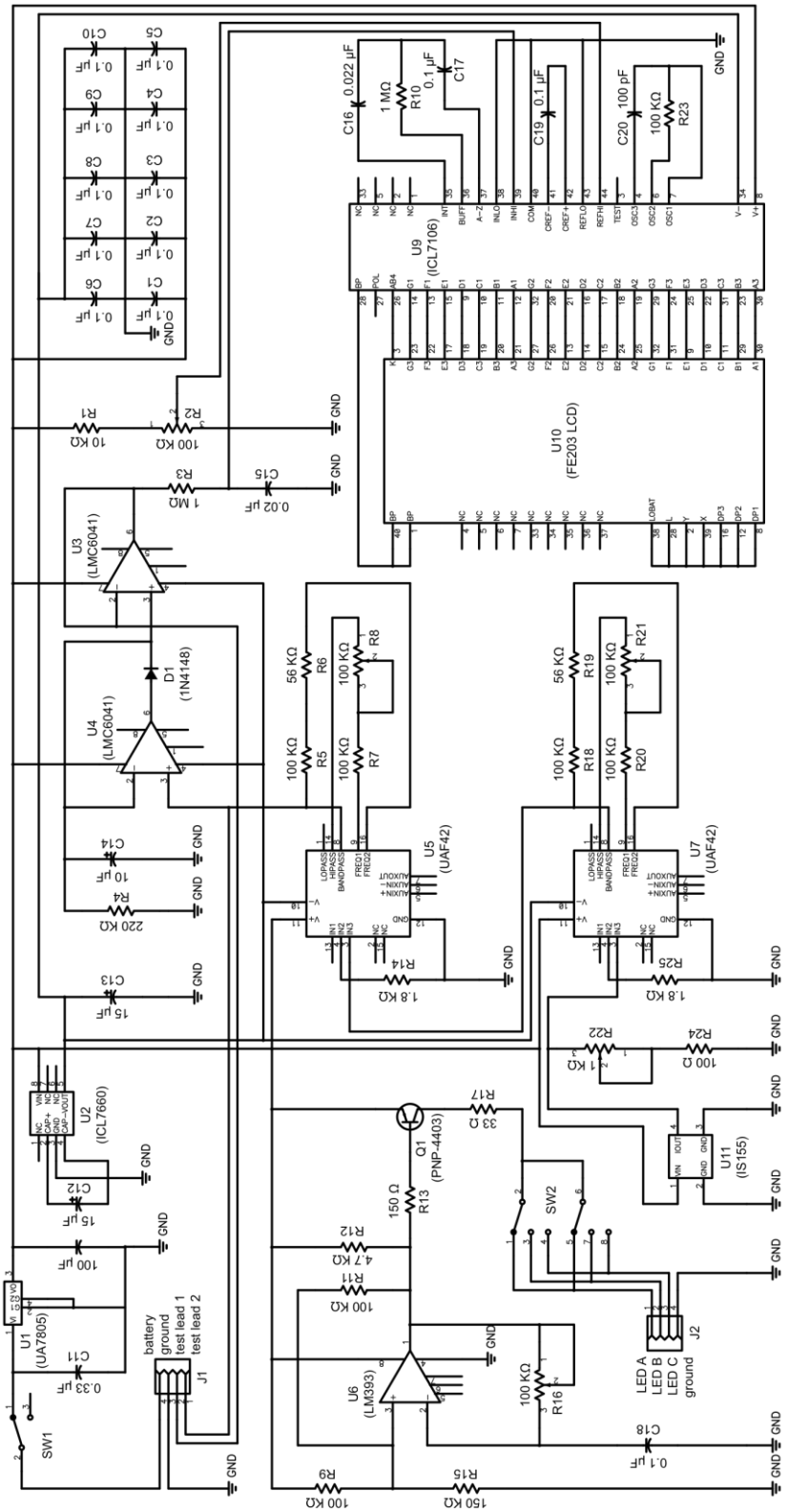
U9 (ICL7106)
U10 (FE203 LCD)
U3 (LMC6041)
U4 (LMC6041)
D1 (1N4148)
U5 (UAF42)
U7 (UAF42)
U2 (ICL7660)
U1 (UA7805)
U6 (LM393)
Q1 (PNP-4403)
U11 (IS155)
SW1
SW2
J1
J2
battery
ground
test lead 1
test lead 2
LED A
LED B
LED C
ground
GND
C16 0.022 µF
C17 0.1 µF
C19 0.1 µF
C20 100 pF
R10 1 MΩ
R23 100 KΩ
R1 10 KΩ
R2 100 KΩ
R3 1 MΩ
C15 0.02 µF
R6 56 KΩ
R8 100 KΩ
R5 100 KΩ
R7 100 KΩ
R19 56 KΩ
R21 100 KΩ
R18 100 KΩ
R20 100 KΩ
R14 1.8 KΩ
R25 1.8 KΩ
R22 1 KΩ
R24 100 Ω
R17 33 Ω
R13 150 Ω
R12 4.7 KΩ
R11 100 KΩ
R16 100 KΩ
R9 100 KΩ
R15 150 KΩ
C18 0.1 µF
C14 10 µF
R4 220 KΩ
C13 15 µF
C12 15 µF
C11 0.33 µF
100 µF
C1 0.1 µF
C2 0.1 µF
C3 0.1 µF
C4 0.1 µF
C5 0.1 µF
C6 0.1 µF
C7 0.1 µF
C8 0.1 µF
C9 0.1 µF
C10 0.1 µF

Figure S-4.

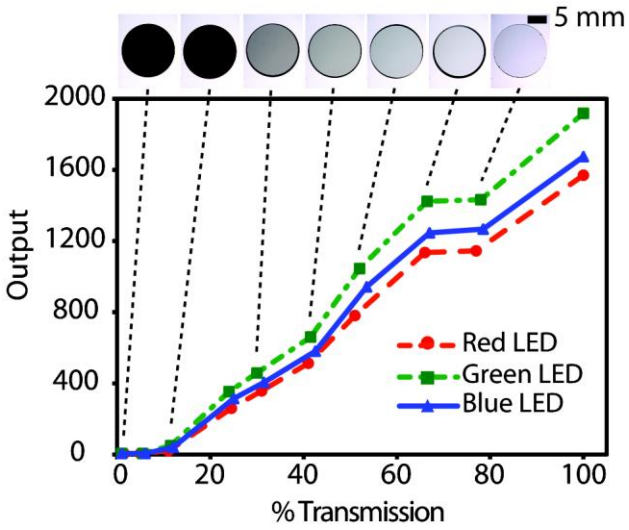
5 mm
2000
1600
1200
800
400
0
Output
0
20
40
60
80
100
% Transmission
Red LED
Green LED
Blue LED

Figure S-5.

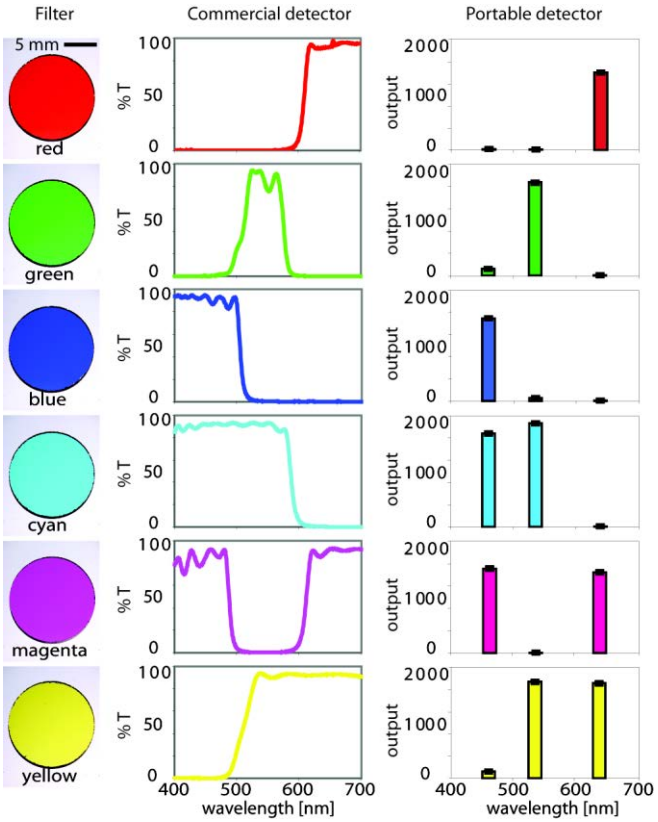
Filter
Commercial detector
Portable detector
5 mm
red
green
blue
cyan
magenta
yellow
% T
output
wavelength [nm]
0
50
100
1000
2000
400
500
600
700

Figure S-6.

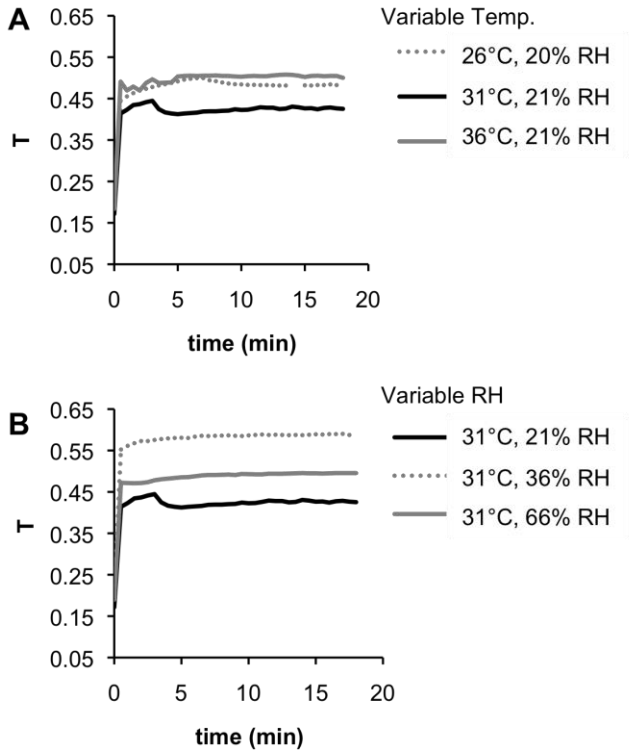
A
0.65
0.55
0.45
0.35
0.25
0.15
0.05
T
0
5
10
15
20
time (min)
Variable Temp.
26°C, 20% RH
31°C, 21% RH
36°C, 21% RH
B
0.65
0.55
0.45
0.35
0.25
0.15
0.05
T
0
5
10
15
20
time (min)
Variable RH
31°C, 21% RH
31°C, 36% RH
31°C, 66% RH

Figure S-7.

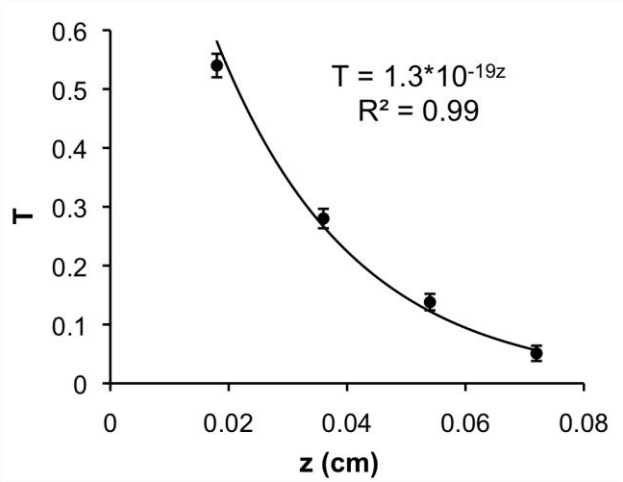

TABLE CAPTIONS

Table S-1. Making paper translucent by applying index-matching fluids. Relationship between type of paper, fluid, and transmission of light through the paper. The index of refraction of the cellulose-based chromatography papers was 1.45–1.62.[11] The values of *T* reflect the averages and standard deviations from seven measurements.

Table S-2. Quantifying the level of bovine serum albumin in artificial urine using transmittance colorimetry under different environmental conditions for a sample in (10 μM) and out (40 μM) of the linear operating range of the assay. Values represent the averages and standard deviations from nine measurements.

Table S-1.

Paper	Thickness (μm)	Fluid	n_{fluid} [a]	T [b]
Whatman Chrom. Paper No. 3	250	none	–	0.00 ± 0.00
		vegetable oil	1.471	0.15 ± 0.02
		PMPS[c]	1.536	0.20 ± 0.07
Whatman Chrom. Paper No. 1	190	None	–	0.09 ± 0.00
		Distilled water	1.34	0.30 ± 0.03
		PDMS[d]	1.404	0.35 ± 0.05
		ethylene glycol	1.431	0.30 ± 0.02
		Mineral oil	1.467	0.53 ± 0.02
		vegetable oil	1.471	0.54 ± 0.02
		PMPS[c]	1.536	0.57 ± 0.04
Technicloth® Wipers	130	None	–	0.14 ± 0.02
		vegetable oil	1.471	0.50 ± 0.0
		PMPS[c]	1.536	0.50 ± 0.1
Scott Roll Towels	20	None	–	0.30 ± 0.0
		vegetable oil	1.471	1.03 ± 0.00
		PMPS[c]	1.536	1.03 ± 0.01
VWR Light-Duty Tissue Wipers	10	None	–	0.40 ± 0.0
		vegetable oil	1.471	1.03 ± 0.00
		PMPS[c]	1.536	1.02 ± 0.01

[a] Refractive index data for mineral oil, distilled water, ethylene glycol, and poly(methylphenylsiloxane) were obtained from Sigma-Aldrich chemical data sheets; poly(dimethylsiloxane) data was obtained from the Polymer Data Handbook, Oxford University Press (1999). [b] We hypothesize that the values listed here consistently overestimate the total transmittance, due to a system flaw that causes a consistent underestimation of I_o. This underestimation would explain why values of ($T > 1$) are obtained for some paper-fluid combinations presented in this table. [c] PMPS: poly(methylphenylsiloxane) [d] PDMS: poly(dimethylsiloxane)

Table S-2.

Lighting	Wind[a]	[BSA] (μM) in artificial urine[b]		
		Actual	Measured	Actual/Measured
overhead fluorescent	none	10	12 ± 3	0.83
dark			10 ± 11	1.00
sunlight			13 ± 4	0.71
overhead fluorescent		40	30 ± 5	1.33
dark			31 ± 10	1.29
sunlight			22 ± 6	1.82
overhead fluorescent	simulated	10	13 ± 8	0.77
dark			5 ± 3	2.00
sunlight			16 ± 4	0.63
overhead fluorescent		40	24 ± 5	1.67
dark			20 ± 5	2.00
sunlight			28 ± 8	1.43

[a] Wind conditions were simulated by acquiring data while the POCKET detector was positioned < 2 ft from an ordinary table fan. [b] The artificial urine solution contained 1.1 mM lactic acid, 2.0 mM citric acid, 25 mM sodium bicarbonate, 170 mM urea, 2.5 mM calcium chloride, 90 mM sodium chloride, 2.0 mM magnesium sulfate, 10 mM sodium sulfate, 7.0 mM potassium dihydrogen phosphate, 7.0 mM dipotassium hydrogen phosphate, and 25 mM ammonium chloride all mixed in Millipore-purified water. The pH of the solution was adjusted to 6.0 by addition of 1.0 M hydrochloric acid.